Bottom-Up Statistical PLC Channel Modeling—Part II: Inferring the Statistics

Andrea M. Tonello, *Member, IEEE*, and Fabio Versolatto, *Graduate Student Member, IEEE*

***Abstract*—We investigate the statistical behavior of power-line communication (PLC) channels. It is inferred from the results obtained with a statistical bottom-up channel simulator (described in Part I of this paper) that uses an in-home topology model derived from the observation of wiring practices and norms. It computes channel transfer functions via the application of transmission-line theory. The comprehensive study includes the analysis of the statistics of the path-loss profile, the average channel gain, the root-mean-square delay spread, and the channel capacity. We highlight the dependency on topological information as the network layout area, the intensity of outlets, the backbone length, etc. We furthermore propose a channel classification based either on average capacity or topological information (e.g., the belonging of outlets to rooms served by the same derivation box). We show that the developed channel simulator constitutes a powerful theoretical framework for the generation and analysis of statistically representative channels with a strong connection to physical reality and close match to the results obtained in the measurements campaigns.**

***Index Terms*—Channel modeling, power-line communications (PLC).**

I. Introduction

POWER-LINE communications (PLC) are gaining great interest from a research/development and a standardization perspective. The development of reliable communication techniques and protocols require the knowledge of the channel statistics and the development of statistically representative channel simulators. Although a lot of literature exists on deterministic channel modeling, statistical modeling has attracted attention only recently [1]–[10]. In [2], an analysis of the channel statistics has been carried out from the results of a measurement campaign of in-home networks presented in [3]. From this set of results, two different top-down statistical phenomenological channel simulators have been proposed in [4] and [5]. More recently, a statistical analysis and a channel simulator have been proposed in [6] starting from the database of measurements collected in [7] according to the methodology explained in [8]. These channel simulators are simple but miss the connection with topological information. An early attempt to include this information has been described in [9] where a bottom-up approach is followed and it focuses on the American indoor scenario. From the observation of wiring practices and norms in Europe, we have presented a statistical topology model for in-home power-line networks in Part I of this work [1]. Then, we have proposed an efficient method to compute the channel transfer function using transmission-line (TL) theory among pair of outlets of a given topology realization. The result is a statistical bottom-up channel simulator that enables fast generation of channel responses and, importantly, it maintains connection with physical reality and topological information.

This paper presents an in-depth analysis of the statistics of the power-line communications (PLC) in-home channel using the simulator in [1] which is a powerful tool that allows inferring the channel statistical behavior. Some preliminary studies have been reported in [10]. The comprehensive analysis of this paper includes the investigation of the statistics of the path-loss profile, the average channel gain, the root-mean-square (rms) delay spread, and the channel capacity. We highlight the dependency on topological information as the network layout area, the intensity of outlets, the backbone length, etc. We furthermore propose a channel classification based either on average capacity or topological information (e.g., outlets served by the same derivation box) or to different clusters.

We also carry out a comparison and show the consistency with the results provided by the analysis of experimental data reported in [3], [7], and [11]. Furthermore, the simulator is capable of representing the overall channel variability which may be overshadowed by the relatively small number of channel realizations (in the order of 200) collected via measurements [3], [6]. Moreover, the analysis of measurements reported in the literature considers the ensemble of collected channels and does not discriminate channels if they belong to networks with a different area, type of wiring, number of outlets, and so on. In this respect, the analysis reported in this paper brings new light to the understanding of the fundamental characteristics of in-home PLC channels and their relation to common wiring practices and topological information.

This paper is organized as follows. In Section II, we briefly recall the aforementioned bottom-up random channel simulator. Section III deals with the analysis of delay spread, average channel gain, and path loss and the dependency of these metrics to the topological features. The channel capacity is studied in Section IV. The conclusions are then reported in Section V.

II. Bottom-Up Random Channel Generator

We consider the statistical PLC channel simulator for in-home networks that we have thoroughly described in the first part of this paper [1]. For the sake of clarity, we herein

Manuscript received February 17, 2010; accepted May 03, 2010. Date of publication August 09, 2010; date of current version September 22, 2010. Paper no. TPWRD-00116-2010.

The authors are with the Dipartimento di Ingegneria Elettrica, Gestionale e Meccanica, DIEGM, Università di Udine, Udine 33100, Italy (e-mail: tonello@uniud.it; fabio.versolatto@uniud.it).

Color versions of one or more of the figures in this paper are available online at http://ieeexplore.ieee.org.

Digital Object Identifier 10.1109/TPWRD.2010.2053561

summarize the main features. It has been implemented following a bottom-up approach starting from a statistical model of in-home topologies. Then, for each topology realization, we compute the channel transfer function among pairs of outlets using an efficient method approach based on transmission-line theory.

The topology model has been derived by the observation of European norms and common wiring practices which shows that the overall layout can be divided in clusters. Each cluster contains a derivation box that gathers the wire connections with the outlets. The derivation boxes are connected among them to distribute the energy from the main panel. Thus, to statistically represent reality, we have proposed partitioning a given topology area A_f in a number of clusters of identical area A_c. The cluster area is assumed to be uniformly distributed in a certain interval $[A_{c_m}, A_{c_M}]$. A derivation box (also referred to as root) is allocated to each cluster and it is positioned in the top-left corner with a random shift. The distance of the root from the top-left corner is denoted with d_r. Then, the outlets of a given cluster are located on the perimeter and are assumed to be drawn from a Poisson arrival process with intensity $\Lambda_o A_c$. The wire connection between the root and the outlets is completed according to a minimum distance criterion and follows with equal probability a bus structure along the perimeter (BP), a star topology with minimum distance (SD), and a star topology with conductors placed along the perimeter (SP). The cable length of the outlet-root connection is denoted by d_l. The roots are directly fed by the main panel or by the nearest root in the direction of the main panel. A set of N_l loads is used. They have been obtained from measurements and are representative of typical lamps and appliances. The probability that an outlet does not have any load is p_v. Finally, different size cables with certain electrical characteristics are used for the root-root and root-outlet connections to take into account that roots need to carry higher currents. The specific set of parameters used is reported in the next section.

The channel transfer function (CTF) among two outlets (i.e., the insertion loss assuming a 50-Ω receiver node impedance) is computed in the frequency domain. The algorithm can be considered as a scalar version of the ABCD matrix method as shown in the Appendix of [1]. It appears to be particularly efficient since it reduces complex networks to a backbone (shortest path among the two considered nodes) with a certain number of equivalent admittances connected in parallel to the backbone. Each admittance is associated to a branch that departs from the backbone. The backbone is divided in units, one per branch or portion of the backbone with homogenous electrical properties. Then, the overall CTF is calculated via the product of the input–output voltage ratio of the units.

III. Channel Statistics

We study the statistics of the channel and, in particular, those of the average channel gain, the path-loss profile, the delay spread, and the channel capacity, taking into account their dependency on the topology parameters.

TABLE I
Simulation Setup of the Bottom-Up Generator for Channel Band 1–30 MHz

Parameter	Values
A_f (m^2)	80, **160**, 240
Λ_o $(outlets/m^2)$	0.1, **0.5**, 1
p_v	0.1, **0.3**, 1
l_{min} (m)	0, **5**, 10
A_f (m^2)	$\mathcal{U}(\mathbf{15}, \mathbf{45})$
N_l	**10**

A. Average Channel Gain

The average channel gain (ACG) for a given CTF realization $H(f)$ is defined as

$$G = 10^{G_{\mathrm{dB}}/10} = \frac{1}{n_2 - n_1} \sum_{i=n_1}^{n_2} |H(iFs)|^2 \qquad (1)$$

where F_s is the sampling frequency resolution and G_{dB} is the ACG in decibels. We choose $F_s = 100$ kHz, $n_1 = 10$, and $n_2 = 300$ (therefore, the 1–30 MHz channel band). The ACG is an important metric since the signal-to-noise ratio (SNR) at the receiver input is a function of it. In fact, assuming a uniform transmit power distribution with spectral density P_x, and white noise with power spectral density N_0, we obtain for a given channel realization $\mathrm{SNR} = GP_x/(N_0 F_s)$.

We carry out a statistical analysis to understand the relations between the ACG and the topology features. In particular, we examine how the ACG is related to the topology area A_f to the intensity per-unit area of the outlets Λ_o, to the probability that no outlets are connected to a plug p_v, and to the minimum length of the backbone $l_{\min}$ (i.e., considering the subset of channel responses associated with outlets whose backbone length is larger than $l_{\min}$).

We focus our attention on each individual parameter. The default configuration of parameters is shown in bold (second column) in Table I. When we study the impact of a specific parameter, we set the others to their correspondent bold values. The cluster area A_c is always considered as a uniformly distributed random variable between 15 and 45 m^2 (as encountered in practice), while the number of considered topology realizations is 1000. As an example, to exploit the impact of the topology area on the ACG, we collect simulations from topologies of area 80, 160, and 240 m^2, generated with a default configuration for the remaining parameters.

In Fig. 1, we plot the quantile-quantile (qq) plots of G_{dB} versus the standard normal quantiles as a function of the parameters. The best normal fit is also shown for every case (dashed lines). More in detail, in Fig. 1(a), we consider three area values, while in Fig. 1(b), we vary the outlet intensity per-unit area, and in Fig. 1(c), we vary the no-load probability. Finally, in Fig. 1(d), we report the results for intracluster and intercluster channels. This classification was introduced in [12]. The former class considers channel realization associated with outlets belonging to the same cluster, while the latter gathers channels between outlets in different clusters. We further recall that a cluster corresponds to a small set of rooms served by the same derivation box. When showing results for inter/intracluster channels, we

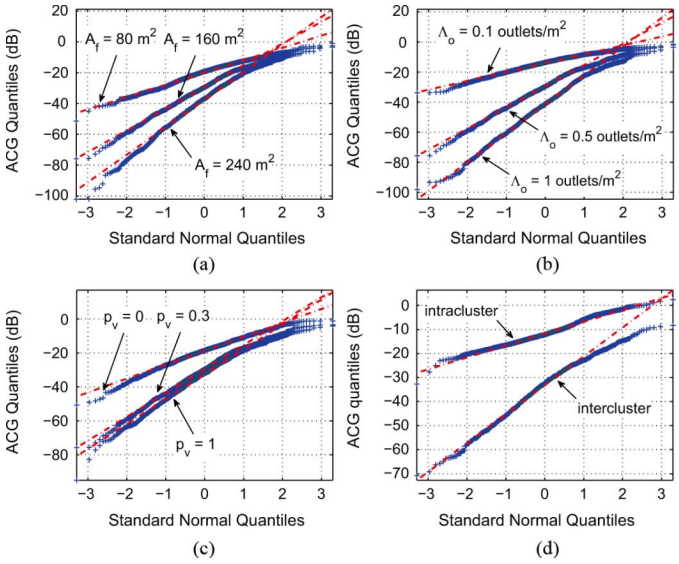

Fig. 1. Average channel gain as a function of: (a) topology area, (b) per-unit area outlet intensity, (c) probability of open outlets, and (d) inter/intracluster channel classes.

modify the default configuration by setting $l_{\min}$ to 0 m in order to avoid any bias especially for intracluster channels that are associated with shorter backbone lengths.

The linear trends observed in almost every plot of Fig. 1, allow us to speculate a log-normal behavior for the ACG. Deviations from log-normality are found for high values (i.e., values close to 0 dB). ACG values larger than 0 are possible since we define the channel transfer function as the insertion loss between the transmitter and receiver outlets.

We report the standard deviation, the minimum, mean, and maximum values of $G_{\rm dB}$ as a function of different parameters in Table II. The first row corresponds to the default set of parameters in Table I. In the other rows, we consider the influence of a parameter at the time, referring to the default configuration for the remaining ones. The second row of Table II shows that as the flat area increases, the minimum value and the standard deviation of $G_{\rm dB}$ rapidly decrease. We justify this behavior, observing that the average backbone length increases in larger topologies. Hence, we expect to find worse average channel gains.

A larger impact on the ACG is found due to an increase in the outlet intensity per-unit area Λ_o as row three of Table II shows along with Fig. 1(b). On the contrary, we have found a minor variation of the ACG as a consequence of a variation of the probability of open outlets p_v.

The analysis of the intra/interclster channels reveals, as intuition suggests, that intercluster channels exhibit worse and more spread ACG than intracluster channels.

B. Path Loss

We define the path loss (PL) as $P(f) = |H(f)|^2$ and its version in decibels as $P_{\rm dB}(f) = 20\log_{10}|H(f)|$ where $H(f)$ is the frequency response (insertion loss) between the transmitter and the receiver.

In Fig. 2(a), we show the quantile-quantile plot of the PL in decibels at frequencies 1, 15, and 30 MHz, versus the standard normal quantiles. We also report the best normal fit (dashed lines).

TABLE II
STATISTICS OF AVERAGE CHANNEL GAIN

		std. var. (dB)	min. (dB)	mean (dB)	max. (dB)
default config.		**13.1**	**−75.7**	**−30.3**	**−3.5**
A_f	80	7.7	−51.4	−20.3	−1
	240	17.3	−102	−38.5	−2.5
Λ_o	0.1	5.7	−33.8	−14.2	−1.9
	1	17.8	−98.1	−42.1	−1.6
p_v	0	14	−94.9	−33.2	−4.1
	1	8.4	−50.7	−19.1	−1.1
l_{min}	0	13.7	−75.7	−29.5	−1.6
	10	12.4	−75.7	−32.4	−4.6
class	intracl.	5	−32.7	−11.6	2.4
	intercl.	11.2	−70.8	−33.7	−8.3

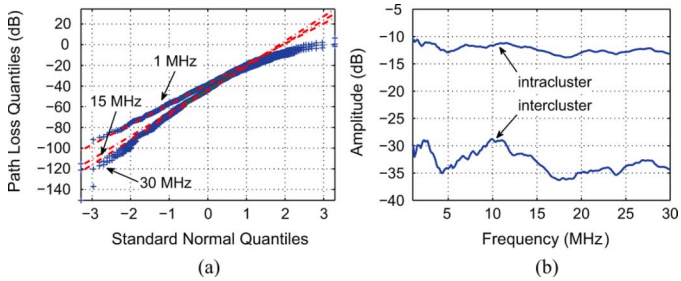

Fig. 2. (a) Quantile-quantile plots of path loss for different frequencies. (b) Average path loss profiles for intercluster and intracluster channel classes.

TABLE III
NULL HYPOTHESIS TESTS FOR THE PATH LOSS $P_{\rm dB}$

	Jarque-Bera	Lilliefors
$P_{dB}(f = 1\ MHz)$	Accepted (0.138)	Accepted (0.186)
$P_{dB}(f = 15\ MHz)$	Rejected	Accepted (0.069)
$P_{dB}(f = 30\ MHz)$	Rejected	Accepted (0.136)

Interestingly, in all three cases, deviations from the standard normal are manifested only for low values of $P_{\rm dB}$ since it has to be lower than 0 dB. In Table III, we report the results of the Lilliefors and Jarque-Bera tests by randomly picking 200 channel realizations. Within brackets, we show the corresponding test probability value. We limit our investigation to 200 realizations only, so that results can be easily compared to those presented in [6]. Tests reveal that for $f = 15$ MHz, the PL in decibels cannot be strictly considered as a normal variable different from the other two cases. However, the best fit for the PL is to use a log-normal distribution as suggested by the experimental evidence [6].

In Fig. 2(b), we report the average PL for the intracluster and intercluster channel classes. Once again as the intuition suggests, the intercluster channels present a worse path-loss profile with regards to the intracluster ones. Fig. 2(b) is helpful to understand how much better intracluster channels behave.

In order to highlight the connections between the path-loss behavior and the wiring structures inside clusters, we show in Fig. 3, the average PL profile in the presence of SD, SP, or BP outlet-derivation box connections. More in detail, we simu-

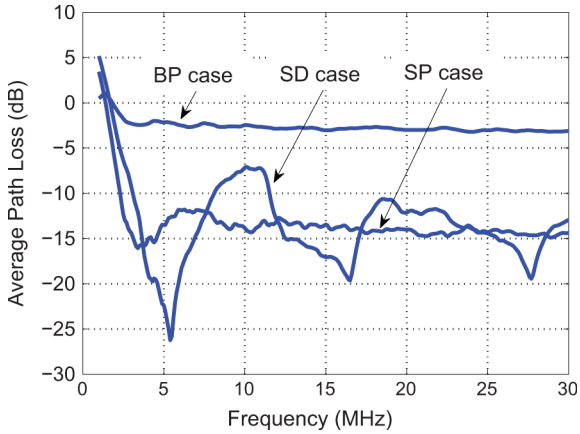

Fig. 3. Average path loss for different wiring connections between derivation boxes and outlets.

late 1000 intracluster channel realizations for each of the three wiring structures. At this scope, we fix $A_c = 30$ m^2 and $p_v = 1$ (i.e., all outlets do not have loads) in order to limit every possible variability not connected to the wiring structure. Fig. 3 shows that when the connections are completed with a bus topology and conductors are placed along the perimeter, namely, the BP case, the PL is less significant. The low level of mean attenuation observed in this case can be explained by the fact that the outlet inter distances are exponentially distributed and this yields, on average, short backbone lengths that introduce less attenuation effects. For the other two cases (SD and SP), we have found more attenuated profiles that are also affected by ripple effects.

C. Delay Spread

The rms delay spread (RMS-DS) is another important parameter for system design. The RMS-DS represents the energy spread of the impulse response. It is defined as

$$\sigma_\tau = \sqrt{\frac{\sum_{i=0}^{N-1} (iT_s)^2 |h_i|^2}{\sum_{i=0}^{N-1} |h_i|^2} - \left(\frac{\sum_{i=0}^{N-1} iT_s |h_i|^2}{\sum_{i=0}^{N-1} |h_i|^2} \right)^2} \qquad (2)$$

where T_s, h_i, and N are the sampling time resolution, the channel impulse response at instant iT_s, and the number of impulse response points, respectively.

Similar to the analysis of the ACG, in the following text, we investigate the relation between the RMS-DS and the topology parameters. We show the delay spread as function of the channel class (intercluster and intracluster), and we study the relation between the RMS-DS and the coherence bandwidth.

Fig. 4(a) shows the cumulative distribution function of the RMS-DS varying the area A_f, while in Table IV, we report the standard deviation, the minimum, mean, and the maximum values. In accordance with experimental results [6], the log-normal distribution is the best fit for all of the CDF profiles, although the RMS-DS is not strictly a log-normal distributed variable as we discuss in more detail in the following text. We also observe that the network area A_f affects the average value of the RMS-DS but does not significantly affect the standard deviation and the minimum/maximum values.

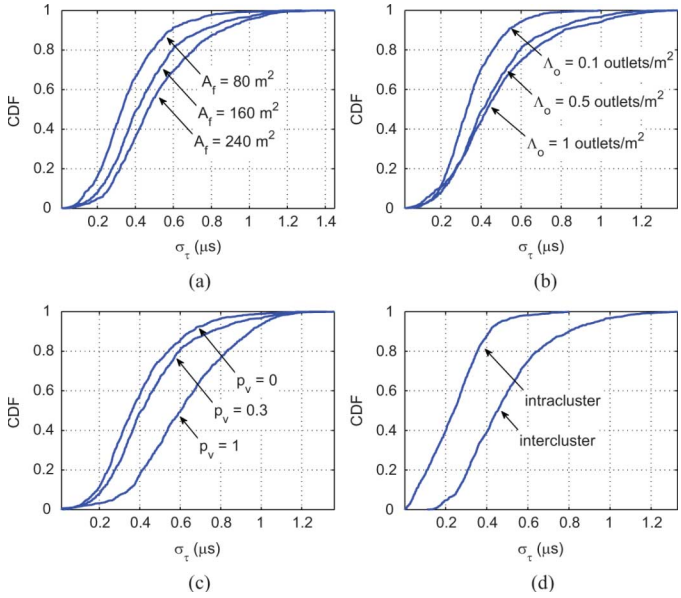

Fig. 4. Delay spread as a function of (a) topology area, (a) per-unit area outlet intensity, (c) probability of open outlets, and (d) inter/intracluster channel classes.
(b) Probability of open outlet. (c) and (d) Inter/intracluster channel class.

TABLE IV
STATISTICS OF THE RMS DELAY SPREAD

		std. var. (μs)	min. (μs)	mean (μs)	max. (μs)
default config.		**0.220**	**0.021**	**0.451**	**1.361**
A_f	80	0.180	0.013	0.360	1.276
	240	0.237	0.022	0.516	1.449
Λ_o	0.1	0.143	0.023	0.351	0.996
	1	0.256	0.02	0.478	1.381
p_v	0	0.193	0.044	0.397	1.298
	1	0.237	0.014	0.619	1.322
l_{min}	5	0.224	0.01	0.442	1.361
	10	0.217	0.055	0.469	1.346
class	intracl.	0.142	0.001	0.243	0.802
	intercl.	0.219	0.112	0.492	1.328

Now, in Fig. 4(b), we consider the effect of the outlet intensity per-unit-area Λ_o that is equal to 0.1, 0.5, and 1. The second row of Table IV shows the mean, the standard deviation, and the minimum and the maximum RMS-DS values observed for these simulations. The results show that while for low intensity values their variations affect the RMS-DS, for Λ_o that goes to one, the RMS-DS flattens out.

Fig. 4(c) and the third row of Table IV report the effect on the RMS-DS as a variation of the probability of open outlets p_v equal to 0, 0.3, and 1. The outlet loads significantly affect the RMS-DS. More in detail, when $p_v = 1$ (all of the outlets are open), we find the worst case. Furthermore, for this case, the RMS-DS is not log-normal any more, but rather it exhibits normal behavior.

Finally, intracluster channels have an RMS-DS that is lower (almost half) than that associated with intercluster channels, as Fig. 4(d) and the last row of Table IV show.

We now investigate further the statistical behavior of the RMS-DS. We consider a subset of the channel responses that

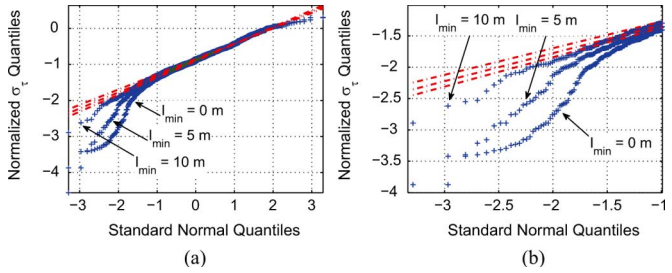

Fig. 5. (a) Qq-plot of the logarithmic normalized delay spread as a function of $l_{\min}$, and (b) its magnification for lower tails (on the right).

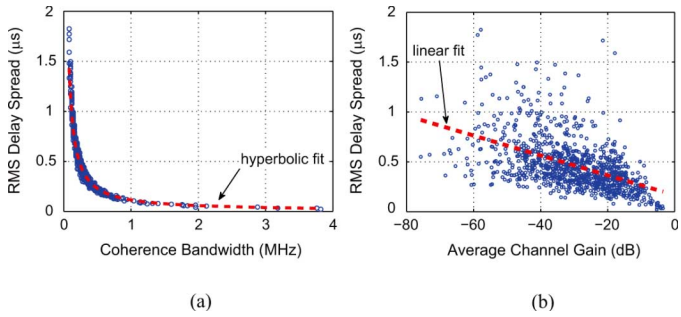

Fig. 6. (a) Delay spread as a function of (a) coherence bandwidth and (b) average channel gain. In both cases, best fits are also shown.

are associated with a backbone length larger than a minimum value $l_{\min}$. We have found that log-normality is a good statistical fit for large values of $l_{\min}$. On the contrary, if we constraint the backbone length to short values, then the RMS-DS statistics diverge from log-normality. This is because when the backbone is short, the channel is less affected by scattering effects. Hence, the claimed log-normality due to the large number of random reflections is no longer valid. The fifth row of Table I reports the RMS-DS values for channels with a backbone longer than 5 or 10 m. In Fig. 5(a), we show the qq plot for the logarithmic RMS-DS defined as

$$\bar{\sigma}_\tau = \log\left(\frac{\sigma_\tau}{10^{-6}}\right) \tag{3}$$

versus the normal distribution. The best normal fit is also shown. The curves point out that $\bar{\sigma}_\tau$ is normal distributed (in agreement with the experimental results [6]) for high values, while for low values, a strong deviation from the normal distribution is encountered. To highlight this behavior, we zoom the qq plot in Fig. 5(b). If the backbone length is not bounded, the RMS-DS can reach very low values down to less than 20 ns. Conversely, when the channel backbone is longer than 10 m, the smallest delay spread is more than 70 ns.

D. Relation Between RMS-DS and Coherence Bandwidth

Now, we want to investigate the relation between the delay spread and the coherence bandwidth. We define the deterministic autocorrelation function (ACF) of the CTF as

$$R(\Delta f) = \int_B H(f+\Delta f)H(f)^* \mathrm{d}f \tag{4}$$

where $H(f)^*$ is the CTF complex conjugate. The ACF allows evaluating the frequency range over which the CTF can be considered flat. In particular, this range is usually referred to as coherence bandwidth B_α and it is defined as twice the frequency range Δf so that $R(\Delta f) \geq \alpha R(0)$, for a coefficient α less than 1. We choose $\alpha = 0.9$ and we report in Fig. 6(a) the RMS-DS versus coherence bandwidth for 1000 channel realizations assuming the default parameters in Table I. For the sake of accuracy, we also use a frequency resolution of 10 kHz.

The figure shows a hyperbolic relation between the RMS-DS and the coherence bandwidth. By fitting the simulation results, we propose the following relation:

$$B_{0.9} = \frac{0.115}{\sigma_\tau}. \tag{5}$$

The result is in excellent agreement with the corresponding ones from the measurements presented in the literature (e.g., [13]).

E. Relation Between RMS-DS and ACG

In Fig. 6(b), we plot the rms delay spread as a function of the average channel gain for each simulated channel (circle marker) assuming the default parameters. Following [6], we look for the best linear fit of the resulting distribution. The slope of the line is equal to -0.0108 μs/dB which matches the results from the analysis in [6] of the measurement campaign in [7]. Essentially, we have found that the RMS-DS decreases when the ACG increases; therefore, worse channels in terms of ACG are also characterized by larger values of RMS-DS.

A comparison with the results in [6] shows that there is a higher number of channels in Fig. 6(b) with lower ACG and RMS-DS than [6, Fig. 4]. This is because the proposed simulator generates all possible channels in a given topology (i.e., all outlet connections are considered comprising those that are very short). On the contrary, the data base of measurements used in [6] is limited and comprises, as described in [8], acquisitions of channels for a pair of outlets that are deliberately chosen to be a probable location where to connect PLC modems. This appears to be restrictive since practical applications may require connection between nearby outlets. To substantiate further this argument, we plot in Fig. 7(a) a sample topology obtained with the default parameter configuration. Then, we choose 10 outlets similarly to what has been done in [8], and we report the RMS-DS versus ACG in Fig. 7(b). The resulting set of channels now exhibits more channels with worse RMS-DS and ACG, and the slope of the best linear fit is still close to -0.01 μs/dB, matching the experimental data in [6] more closely. These results highlight how the arbitrary choice of the outlets in measurement campaigns affects the statistics. Furthermore, the area of the considered topologies has also an effect as discussed in Section III-A. In fact, the experimental data in [7] have been obtained in American houses of an area up to 335 m^2. The corresponding channels have worse ACGs than those reported in [11] for the European context where houses present approximately 80% of channels having an ACG of -50 dB and 50% having ACGs smaller than -35 dB. Hence, exploiting the relation between the ACG behavior and the flat area highlighted in Section III-A, we speculate the existence of a smaller value for the European average topology area. A conclusion also justifies

the area values considered herein for the statistical characterization of European power-line channels.

IV. Capacity

Although delay spread and average channel gain offer a quite complete overview of the power-line channel properties, we also carry out a statistical analysis of channel capacity. At this scope, we recall the Shannon capacity definition that reads

$$C = F_s \sum_{i=n_1}^{n_2} \log_2 \left(1 + \frac{|H(iF_s)|^2 P_T}{P_N}\right) \tag{6}$$

where P_T and P_N are the power spectral density (PSD) of the transmitted signal and the PSD of the considered additive white Gaussian noise. More in detail, we have chosen $P_T = -50$ dBm/Hz and $P_N = -140$ dBm/Hz. We consider the same simulator configurations as in the previous sections. The channel band is 1–30 MHz. The upper capacity bound is approximately equal to 900 Mb/s. We have then divided the capacity interval 0–900 Mb/s into four classes, each with a 225-Mb/s difference to obtain four average values according to Table V.

This classification is similar to the one proposed in [2], but in that case, nine classes are defined and the bandwidth is up to 100 MHz. In Table VI, we report the percentage of channels that fall within a certain class as a function of the simulator parameters.

Table VI shows that as the network area A_f or the outlet intensity Λ_o increases, the capacity decreases so that higher capacity classes are more probable. The capacity is less affected by p_v and $l_{\min}$. Finally, while intracluster channels are confined to the best capacity classes, namely, class 1 and 2, the intercluster channels show a more spread behavior that falls within classes 2 down to 4.

A. Average Path-Loss Profiles of Capacity Classes

We show in Fig. 8 the average path-loss profile for each capacity class of Table V. Channels have been generated with the default configuration of the simulator. We refer to these profiles as "default." Strong ripple effects are present, in particular, for the worst classes, such as class 3 and 4. A deeper investigation has pointed out that the ripples are strongly connected to the derivation box position. To show this, in Fig. 8, we report the path-loss profiles obtained with the default parameters configuration but with the derivation boxes exactly placed in the upper-left corner of each cluster (fixed roots), or with derivation boxes placed anywhere inside the cluster (free roots). The two solutions differ for the maximum value of d_r, which is 0 and $\sqrt{2A_c}$ for the fixed-roots and free-roots cases, respectively. The curves show that for the free-root case, the ripple effects are of lower intensity. However, we believe that regular structures with limited variations of the location of the derivation boxes exist in real layouts, as in office buildings or hotels. Therefore, in these cases, ripple effects in the path-loss profile are exhibited as has also been reported in [14].

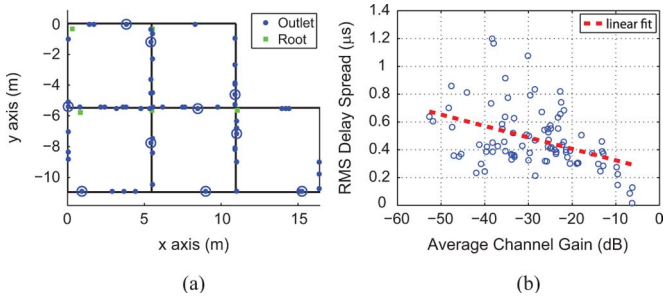

Fig. 7. (a) Randomly generated topology layout where ten outlets highlighted with circles have been selected, and (b) the plot of rms delay spread as a function of the average channel gain for the evaluated channels (on the right). The best linear fit is also shown.

TABLE V
Capacity Intervals

Class	Average Class Capacity (Mb/s)
1	787.5
2	562.5
3	337.5
4	112.5

TABLE VI
Statistics of Capacity

		class 1 (%)	class 2 (%)	class 3 (%)	class 4 (%)
default config.		**6.3**	**43.6**	**37**	**13.1**
A_f	80	15.5	69.7	14.6	0.2
	240	3.4	29.3	35.9	31.4
Λ_o	0.1	40.1	56.5	3.4	0
	1	2.7	24.5	38	34.8
p_v	0	4.9	42	38.7	14.4
	1	2.7	24.5	38	34.8
l_{min}	5	55.4	44.5	0.01	0
	10	2.8	40.6	41.9	14.7
class	intracl.	55.4	44.5	0.01	0
	intercl.	1.2	38.7	46.6	13.5

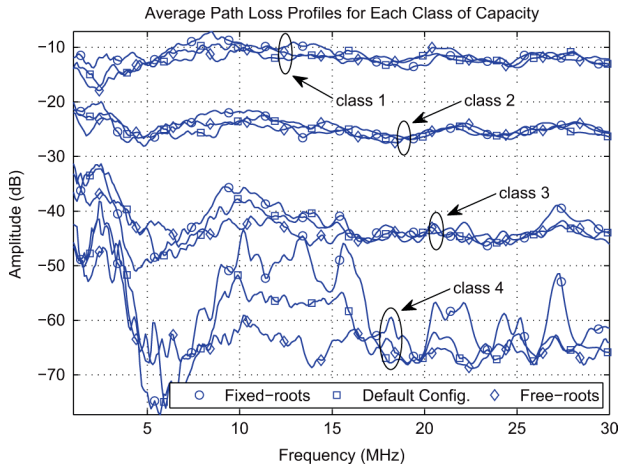

Fig. 8. Average path-loss profiles for each class of capacity.

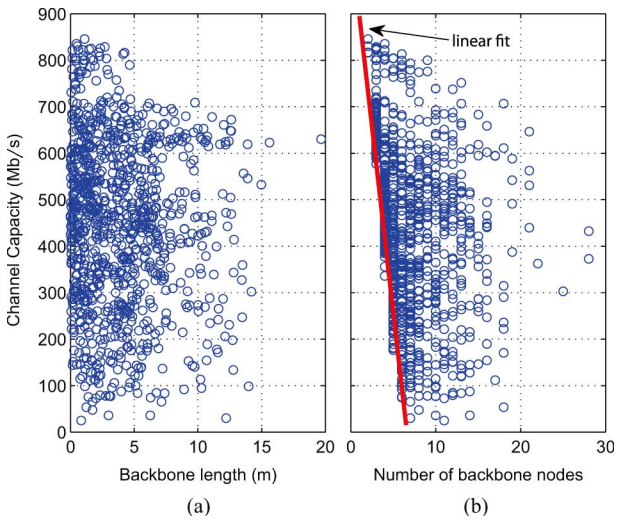

Fig. 9. Plots of the channel capacity in relation to (a) the backbone length and (b) the number of junction nodes of the backbone.

B. Capacity Versus Backbone Features

In order to fully investigate the channel capacity behavior as a function of the topology layout, we report in Fig. 9(a) the capacity achieved by 1000 channel realizations as a function of the associated backbone length. We assume the default parameters configuration with $l_{\min}$ set to 0 m. The plot shows that the backbone length does not influence capacity.

On the contrary, we have found that the number of junction nodes, where branches depart from the backbone, have a larger influence on capacity. This is shown in Fig. 9(b). Interestingly, we have found that the lower capacity bound has a linear trend with the number of backbone junction nodes $n_{\rm bb}$ as follows:

$$C_{\rm bound} = -160 \cdot n_{\rm bb} + 1055 \quad n_{\rm bb} < 7 \tag{7}$$

where $C_{\rm bound}$ is the lower bound of capacity in megabits per second.

V. Conclusion

We have presented a statistical analysis of the in-home power-line communications channel using the bottom-up simulator presented in [1]. The simulator is intrinsically related to physical reality and topology characteristics. It allows inferring the statistics as a function of the topology parameters (e.g., the network area, the backbone length, the outlet number, and the loads). To this respect, the study provides new understandings of the fundamental PLC channel characteristics and their connection to the topology. The results are in good agreement with those obtained from measurement campaigns. In particular, we have shown that the average channel gain and the rms delay spread can be approximately fitted with a log-normal distribution. Deviations from it are found for extreme values and if we constrain the backbone length to be small. It should be noted that the results from measurement campaigns do not discriminate among the topology features and do not consider the whole set of outlets but rather acquisitions have been made among nodes at large distance. To this respect, we have investigated the behavior of channels belonging to the same cluster or to different ones. Finally, we have classified channels according to their capacity as a function of the backbone length and the number of intermediate backbone nodes. While we have not found any strong dependence of capacity from the backbone length, we have found an interesting linearly decreasing dependency between the lower capacity bound and the number of junction nodes in the backbone.

In conclusion, the proposed channel simulator is capable of generating statistically representative channels. It can be parameterized so that it models the behavior of a certain application scenario (e.g., a small/large home or office), characterized by a certain topology.

References

[1] A. M. Tonello and F. Versolatto, "Bottom-up statistical PLC channel modeling—Part I: Random topology model and efficient transfer function computation," *IEEE Trans. Power Del.*, 2010, submitted for publication.

[2] M. Tlich, A. Zeddam, A. Moulin, and F. Gauthier, "Indoor power-line communications channel characterization up to 100 MHz—Part II: Time-frequency analysis," *IEEE Trans. Power Del.*, vol. 23, no. 3, pp. 1402–1409, Jul. 2008.

[3] M. Tlich, A. Zeddam, A. Moulin, and F. Gauthier, "Indoor power-line communications channel characterization up to 100 MHz–Part I: One-parameter deterministic model," *IEEE Trans. Power Del.*, vol. 23, no. 3, pp. 1392–1401, Jul. 2008.

[4] A. M. Tonello, "Wideband impulse modulation and receiver algorithms for multiuser power line communications," *EURASIP J. Adv. Signal Proces.*, vol. 2007, pp. 1–14.

[5] M. Tlich, A. Zeddam, A. Moulin, F. Gauthier, and G. Avril, "A broadband powerline channel generator," in *Proc. IEEE Int. Symp. Power Line Commun. App.*, Mar. 2007, pp. 505–510.

[6] S. Galli, "A simplified model for the indoor power line channel," in *Proc. IEEE Int. Symp. Power Line Commun. App.*, Apr. 2009, pp. 13–19.

[7] B. O'Mahoney, A. Garrett, M. Wilson, and P. Rajkotia, "Powerline channel data," contribution to ITU-T SG15Q4 WG, 2007, ser. B07 0515 (NIPP NAI 2007 107R1), Geneva, Switzerland.

[8] B. O'Mahony, "Field testing of high speed power line communications in North American homes," in *Proc. IEEE Int. Symp. Power Line Commun. App.*, Mar. 2006, pp. 155–159.

[9] T. Esmalian, F. R. Kschischang, and P. G. Gulak, "In-building power lines as high-speed communication channels: Channel characterization and a test channel ensemble," *Int. J. Commun. Syst.*, vol. 16, pp. 381–400, 2003.

[10] F. Versolatto and A. M. Tonello, "Analysis of the PLC channel statistics using a bottom-up random simulator," in *Proc. IEEE Int. Symp. Power Line Commun. App.*, Mar. 2010, pp. 236–241.

[11] ETSI, Hidden node review and statistical analysis, Power Line Telecommunications (PLT), TR102 269, 2003.

[12] A. M. Tonello and F. Versolatto, "New results on top-down and bottom-up statistical PLC channel modeling," in *Proc. 3rd Workshop on Power Line Communications and its Applications*, Oct. 2009, pp. 11–14.

[13] J. A. Cortés, L. Díez, and J. T. Entrambasaguas, "Characterization of the cyclic short-time variation of indoor power-line channels response," in *Proc. IEEE Int. Symp. Power Line Commun. Its App.*, Apr. 2005, pp. 326–330.

[14] S. Tsuzuki, S. Yamamoto, T. Takamatsu, and Y. Yamada, "Measurement of japanese indoor power-line channel," in *Proc. IEEE Int. Symp. Power Line Commun. App.*, Apr. 2001, pp. 79–84.

Andrea M. Tonello (M'02) received the D.Eng. degree in electronics (Hons.) and the Doctor of Research degree in electronics and telecommunications from the University of Padova, Padova, Italy.

In 1997, he joined Bell Labs—Lucent Technologies as a Member of Technical Staff, where he worked on the development of baseband algorithms for cellular handsets, first in Holmdel, NJ, and then within the Philips/Lucent Consumer Products Division, Piscataway, NJ. From 1997 to 2002, he was with the Bell Labs Advanced Wireless Technology Laboratory, Whippany, NJ. He was promoted in 2002 to Technical Manager and was appointed Managing Director of Bell Labs, Italy. Within this role, he has been involved in the standardization activity for the evolution of second- and third-generation cellular technology. In 2003, he joined the Dipartimento di Ingegneria Elettrica, Gestionale, e Meccanica (DIEGM) of the University of Udine, Udine, Italy, where he is an Aggregate Professor and Founder of the wireless and power-line communication lab (WiPLi Lab). He is the co-author of many papers, patents, and standard contributions. He is an Associate Editor for IEEE TRANSACTIONS ON VEHICULAR TECHNOLOGY.

Dr. Tonello received a Lucent Bell Labs Recognition of Excellence award for his work on enhanced receiver techniques in 2003, the award for the best paper published in the *Eurasip Journal on Advances in Signal Processing* about ultra wideband power-line cormmunications (PLC) communication in 2007, and was the coauthor of the best student paper award at IEEE ISPLC 2010. He was co-recipient of two awards in the business plan competition Startcup 2007 and 2008 in Udine. He has been TPC Co-Chair of the IEEE International Symposium on Power Line Communications (ISPLC) 2007, TPC Co-Chair of the general symposium at Globecom 2008, Co-Chair of the track on satellite and positioniong systems at VTC in 2010, the Chair of the Workshop on Power Line Communication 2009, and the Chair of IEEE ISPLC 2011. He is the Vice-Chair elected to the IEEE Technical Committee on PLC.

Fabio Versolatto (GSM'10) received the Laurea (Hons.) and the Laurea Specialistica degrees in electrical engineering (Hons.) from the University of Udine, Udine, Italy, in 2007 and 2009, respectively, where he is currently pursuing the Ph.D. degree.

His research interests are power-line communication channel modeling and digital communication algorithms.

Mr. Versolatto received the award for the best student paper presented at IEEE ISPLC 2010.